Design of micro radial turboexpanders for ORC power cycles: from 0D to 3D

Daniele Fiaschi[(1)], Gianmaria Innocenti[(1)], Giampaolo Manfrida[(1)], Francesco Maraschiello[(2)]

[(1)] Dipartimento di Ingegneria Industriale – DIEF

University of Florence

Viale G. Morgagni, 40-44 – 50135 Florence, ITALY

[(2)]GE Oil & Gas

Nuovo Pignone S.r.l.

Via Felice Matteucci, 2 – 50127 Florence, ITALY

Abstract

The 3D design and analysis of a 5 kW micro turbo expanders for small, distributed ORC power units is proposed, starting from a recently developed 0D design tool, which was initially applied to 50 kW radial turbines.

The turbine was sized referring to R134a as working fluid. At the same time, the main performance parameters, kinematic conditions and the different loss sources were determined. The resulting 0D basic geometry and the related non-dimensional parameters were used as the starting point to define the 3D geometry of the rotor (distribution of the metal blade angles and of the thickness profile) and to refine some design parameters like the number of blades.

On the basis of the 3D blade profile and flow channels, a computational grid was generated. The CFD analysis of the rotor was carried out by means of Ansys Fluent® software, including a real-gas Equation Of State (EOS) model for the working fluid.

The design of the rotor was reconsidered as a consequence of the 3D CFD approach. Finally, the comparison between the 0D and 3D results was carried out, showing a good agreement between the two approaches and, thus, verifying the reliability of the combined 0D – 3D design tool for micro-size turboexpanders of ORCs.

Keywords

ORC Expander, Micro Radial Inflow Turbine, 0D – 3D Turbine Design, Blade loading , Turbine losses

1. Introduction

Research, development and commercialization of Organic Rankine Cycles (ORC) have been in strong growth over the last years, in consequence of the increasing demand of energy recovery from low-value resources (like, for example, low temperature heat sources in the 90 – 200 °C range). The ORC technology is suitable and reliable for mini and micro Combined Heat and Power applications (CHP), with special reference to low size (from a few tens to some hundreds kW). ORCs have a wide range of potential applications as low grade heat recuperators, such as industrial heat waste, renewables and even domestic applications like internal combustion engines [1, 2], solar and geothermal resources [3 – 8]. However, micro-scale ORC based CHP units (< 10 kWel), having a great potential to meet buildings energy demand, have not yet demonstrated their applicability at experimental and commercial level [9].

Only a few studies are found in the technical literature about this small power size, many of which are focused in the selection of the working fluids and in assessing the most suitable expander technologies [10]. Most researchers focus on scroll expanders, which are usually adapted from compressors for refrigeration equipment. This solution is certainly interesting: however, its potential is limited, both in terms of achievable efficiency (usually less than 60%), and of other unfavorable issues such as leakages and, due to the large wetted surface, friction and heat transfer losses [11]. Similar negative issues affect other types of volumetric expanders like the screw ones. In this field of technology, systems for cost effective power production at outputs within the range of 20 – 50 kWe were developed, whereas micro – scale screw expanders (< 10 kWe) are difficult to achieve in the current market. For example, Ormat and ElectraTherm commercialize ORC equipped with these expanders in the range of 50+ kWe [10].

The development of a micro-scale dynamic expander represents a major challenge. Dynamic expanders have proven to be reliable and able to achieve high efficiencies in larger sizes (typically, higher than 50 – 100 kWe [10]): in order to extend their field of application to micro-scale for distributed energy conversion systems, a preliminary screening is certainly needed, assessing issues such as rotational speed, sizing and manufacturing. These are among the main reasons behind the present work.

Literature lacks of modelling and/or experimental studies to assess the design feature and operating issues of micro turbo expanders within kW scale, which is a field typically covered by volumetric machines like scrolls, screw and reciprocating units [10]. Recently, Rahbar et al. [12] proposed a methodology for the preliminary and refined design of radial turbines for low power capacity, coupling mean-line modelling and CFD analysis. Anyhow, their calculations were referred to air as working fluid. Successively, Rahbar et al. [13] presented a novel approach for modelling and optimization of ORC based on a small-scale radial turbine. It merges the ORC cycle with the mean-line modelling of radial inflow turbine combined with integrated optimization technique, but is applied to a 40 – 100 kW size range.

In the following, a design procedure for micro radial ORC turbines (kW class size) is introduced, starting from a 0D tool for the basic sizing (initially applied to a 50 kW turbine) and then using a 3D approach to refine the design by (i) improving the blade geometry and (ii) redefining the most accurate number of blades, in order to achieve a proper blade loading and a good flow guidance thus maximizing the performance of the impeller. Moreover, the CFD calculation of the rotor is useful to validate the actual downscale potential of the developed 0D code, and the limits in the scalability of the different types of losses. The results of the basic 0D and the refined 3D design procedures were compared to validate the ability of the 0D model to provide a reliable preliminary design of the rotor.

2. Preliminary design with 0D model

The first step of the design process is carried out using a 0-D model [14, 15], which guides the user to perform a preliminary sizing of the radial expander evaluating its performance, considering several possible ORC working fluids and rotor geometries (i.e. radial and backswept blades). Reference [14] contains the fundamental guidelines for the correct choice of the main non-dimensional design parameters, such as the *Work coefficient* (Ψ), *Flow coefficient* (Φ), and *Degree of reaction* (R); a second set of non-dimensional geometrical parameters, derived from the fundamental reference literature [16, 17, 18], helps to produce a reasonable design of the machine. In order to facilitate the reader, the main steps are here shortly summarized.

The preliminary sizing and calculation of the turbine geometry is started using the basic input data (rated power output, thermodynamic in/out conditions) and a set of non-dimensional parameters chosen by the designer within a reasonable range, on the basis of the fundamental literature references, having in mind the achievement of a small rotor diameter and a reasonable rotational speed. The choice of the degree of reaction (R_s) is driven on one hand to achieve the energy conversion in one single stage (thus high values would be preferred), on the other hand to limit sealing problems even with open rotor design, relatively economic to manufacture with common machining or precision casting given the low size (low values of reaction degree are preferable in this view). At the same time, high values of the stage loading (ψ) and of the flow coefficient (ϕ), compliant with maintaining the flow in a high subsonic or transonic regime, are selected whenever possible.

This first step allows to select the load and flow coefficients ($\psi=\Delta h_0/u_2$ and $\phi=c_{m2}/u_2$ respectively) and the Isentropic degree of reaction R_s; the acceptability of the fundamental parameters (Specific Diameter and Specific Speed) is also evaluated using the Balje Chart, that gives a reliable indication of the suitability of chosen design parameters. Referring to figure 1, it is further possible to define some non-dimensional geometrical parameters: the nozzle ratio D_1/D_2, the rotor ratio D_3/D_2, the diffuser ratio D_4/D_3, the Diffuser length – diameter ratio L_d/D_3, the Rotor Aspect Ratio b_2/D_2, the Nozzle Height Ratio b_1/b_2. Then, the geometry of the vaned stator (IGV) is determined, as well as its number of blades.

A major issue in rotor design is the choice of the number of blades (Z_B), which deeply affects the rotor geometry and the related losses. The existing literature applies correlations similar to Zweifel's load criterion [16, 17] to calculate Z_B; however, these were developed for large-size machines (often for completely different fluids and originally for axial-flow turbines), so that they become unreliable when applied to downscaled prototypes such as here proposed. The result is typically a high number of blades, and consequently an excessive solidity, and difficulties in manufacturing.

For this reason, it was decided to leave Z_B as a further input design variable, whose value should be chosen from a reasonable compromise between an effective guidance of the fluid through the vanes and a sufficiently low value of the losses between the wet surfaces. The idea was to adjust Z_B after an evaluation of the detailed CFD results. After Z_B is defined, the conditions for optimal incidence at rotor inlet can be defined applying proven correlations [16, 17].

The subsequent step of the 0D design process is the evaluation of the expander losses and their effects on the efficiency of the expansion. Specifically, the relationships of losses with the non-dimensional design parameters (b_2/D_2, ϕ, ψ and R_s) are determined: the contributions include rotor incidence, skin friction, tip clearance, blade loading, disk friction and diffuser losses. The sensitivity of turbine losses and efficiency to ϕ, ψ and R_s leads to a reasonably efficient preliminary 0D design, which is the starting point for the 3D design refinement process.

With respect to the previous work of the Authors [14], the expander is downsized to 5 kW and the related implications in terms of losses and performance are assessed. The key dimensional variable of the 0-D design is the rotor *Inlet diameter* (d_2), together with the thermodynamic data for *inlet total pressure* (p_{01}) and *inlet total* *temperature* (T_{01}). The list of the dimensional and non-dimensional design parameters, referred to the sketch of figure 1, is shown on table 1.

The first-attempt choice was a rotor with 8 backswept blades, which was sized by the 0D model, based on the data available on table 1 and using R134a as the working fluid. The main resulting design data are shown on table 2.

The results of the design exercise for the 5 kW turbine are compared in the following with those of the previous 50-kW class unit. The main issues are:

- the mass flowrate decreases from 1.749 kg/s (50 kW) to 0.1984 kg/s (5 kW), less than linearly due to the different degree of reaction, blade loading and flow coefficient. In particular, the downscaled version has a higher load coefficient (ψ) and a lower flow coefficient (ϕ).
- The rotational speed is more than doubled, passing from 40,000 rpm to about 88,000 rpm, essentially because of the reduction of the rotor diameter (which is less than halved); this result agrees with the typical values of micro expanders reported in literature [13, 15].
- The overall loss coefficient is almost doubled, mainly due to the secondary flows resulting from the increased blade loading. The other sources of losses, like incidence, skin friction, tip clearance, disk friction and profile curvature, are less relevant, as can be seen in the pie-chart diagram of Figure 2 showing the distribution of the rotor losses.
- The resulting total-to-static efficiency of the downsized 5 kW expander is about 8 % points lower (from 0.77 for the 50 kW turbine, to 0.69 for the 5 kW one). This value is in agreement with recently available literature data on radial micro-turbines [13, 15, 19, 20].

3. 3D design procedure: meshing and CFD

The verification of the design procedure by means of CFD was limited to the rotor, which is recognized as the critical component both for performance and technological challenge. The geometry resulting from the 0D preliminary design was transferred into Ansys BladeGen® [21], including blade heights, radii and characteristic angles at the inlet/outlet sections. The geometry of the meridional channel was defined using typical shapes documented in the literature [16, 17] for radial turbines, which were non-dimensionalized and parametrized as a function of the Specific speed N_s (i.e. *Balje chart*). Furthermore, in order to define the internal geometry of the impeller, the distributions of the blade angles have to be defined; the blade angle (β) and the wrap angle (Θ) are in the following relationship:

$$\tan\beta = \frac{d\theta}{dm} \tag{1}$$

where *m* is the meridional coordinate. As a first attempt, a linear distribution of β was considered; the choice of the β – m function, as well as the geometry of the meridional channel, allows the calculation of ϴ by the integration of Eq. (1).

Another relevant feature for the rotor design is the distribution of thickness along the camber line; here, a modified 4 digit series NACA profile (NACA 0005-55) was selected, symmetrical with reference to the mean line and having the maximum thickness located at 50% of the camber line. The resulting CAD 3D model of the impeller is shown in Figure 3.

In order to perform the CFD analysis of the turboexpander, the following step is the generation of a suitable computational grid. The discretization of the domain heavily affects the quality of the solution, both in terms of accuracy and computational costs. As a compromise between these two parameters, a mesh of 991,260 hexahedral elements was created by means of Ansys Turbogrid® software [22]. The structured 3D mesh used in the simulations is shown in Figure 4 (representing the single blade passage which was used for the calculations). In the zone near to the blade surface and walls (hub and tip) the grid was refined; in order to maintain a good compromise between solution accuracy and computational costs, the first cell dimension *y* was defined assuming a target *Dimensionless Wall Distance y+* of about 40 with a *Reynolds Number* of flow close to $3e10^6$. These choices are in accordance to the adopted *k-ω* Turbulence model [23].

The software package Ansys Fluent® [23] was used to perform the computational analysis of the IFR turbine, selecting the model options described in the following.

Numerical Model: steady-state 3D viscous, single phase, compressible flow is used; due to the mesh elements type and topology, a first order upwind advection scheme was chosen because of its numerical stability, as suggested by [24]. Simulations were carried out using a RANS approach (Reynolds Averaged Navier Stokes equations), with the *standard k-ω* turbulence model and the *Density-Based* solver. *Standard k-ω* is an empirical model based on transport equations for the *turbulence kinetic energy* (*k*) and the *specific dissipation rate* (*ω*). The transport equations implemented to achieve the *turbulent kinetic energy k* and the *specific dissipation rate ω* are the following:

$$\frac{\partial}{\partial t}(\rho k)+\frac{\partial}{\partial x_i}(\rho k u_i)=\frac{\partial}{\partial x_j}\left(\Gamma_k\frac{\partial k}{\partial x_j}\right)+G_k-Y_k+S_k \tag{2}$$

$$\frac{\partial}{\partial t}(\rho \omega)+\frac{\partial}{\partial x_i}(\rho \omega u_i)=\frac{\partial}{\partial x_j}\left(\Gamma_\omega\frac{\partial \omega}{\partial x_j}\right)+G_\omega-Y_\omega+S_\omega \tag{3}$$

In order to accurately represent the behaviour and properties of the working fluid (R134a) assumed in the simulations, the cubic Soave-Redlich-Kwong (SRK) Equation of State was activated [25]. The coefficients are given for each equation of state as a function of *critical temperature* T_c, *critical pressure* p_c, *acentric factor* a_f, and *critical specific volume* v_c. The physical properties of R134a are listed in Table 3.

Boundary Conditions (BC): first of all, the computational domain was suitably extended outside of blades area (figure 4), upstream of the *Leading Edge* (LE) and downstream of the *Trailing Edge* (TE), in order to avoid spurious reflections; the extension was about 10% and 50% of the chord length at inlet and outlet respectively. As the computation involved only the rotor, a Single Reference Frame (SRF) calculation was implemented, covering the entire domain; the rotational speed was set at the value provided by the preliminary 0D design. The mass flow rate, total temperature and inlet velocity components calculated by the 0D model were assumed as known inputs of the 3D model at the rotor inlet; their uniform local values at the upstream inlet of the domain were determined by applying the mass, momentum and Rothalpy conservation equations. The setup of the mass flow rate inlet boundary condition required some attention; in fact, the 0D model design gives the flow parameters corresponding to the blade leading edge, whereas the CFD domain is extended upstream. In the definition of boundary conditions, this effect must be taken into account and the flow direction must be assigned in order to obtain the correct value at the leading edge. In practice, there is an extended region of unguided, rotating channel upstream of the actual expander inlet. Within this region, a considerable variation of the velocity components takes place, which is relevant in this case (and generally for this kind of turboexpanders), characterized by a considerable variation of the radial coordinate from the upstream inlet to LE section and by a high rotational speed of the impeller (a consequence of the very small size). The calculation of the flow direction is done applying the mass balance, free vortex and Conservation of Rothalpy equations, respectively:

$$\rho_2 r_2 w_{m2} = \rho_i r_i w_{mi} \tag{4}$$

$$r_2 c_{u2} = r_i c_{ui} = constant \tag{5}$$

$$h_2 + \frac{1}{2} w_2^2 - \frac{1}{2} u_2^2 = h_i + \frac{1}{2} w_i^2 - \frac{1}{2} u_i^2 \tag{6}$$

where the subscript *i* represents the upstream inlet section.

The applied boundary conditions for the simulations are:

- Mass Flow ($\dot{m}$), Flow direction and Total Temperature (T_{02}) at the inlet;
- Static Pressure (p_3) at the outlet;
- Rotational Periodicity at the lateral interfaces;
- Rotational, adiabatic wall for the blade and hub surface

4. Results of the ***first-attempt*** 3D design

The purpose of the simulations for the "first attempt" geometry, was the qualitative evaluation of the impeller flow conditions in order to develop a modified impeller geometry with improved performance. Already in this phase of the procedure, a comparison between the two design approaches (0D and 3D CFD) can be performed in order to assess the issues and reliability of the 0D model and providing, at the same time, a gross check of the 3D calculations. Table 4 reports the main results achieved by the numerical 3D simulations, whereas table 5 shows the comparison between 0D and 3D CFD design for the first attempt geometry.

The power output P was calculated by the total enthalpy drop across the rotor (3), using the mass-weighted average values of enthalpy obtained from the CFD analysis, evaluated at the LE and TE sections.

$$P = \dot{m}(h_{02} - h_{03}) \tag{7}$$

The isentropic Total-to-Static efficiency of the rotor was calculated as:

$$\eta_{ts} = \frac{h_{02} - h_{03}}{h_{02} - h_{3is}} \tag{8}$$

Which represents the ratio between the actual and the maximum theoretical specific work of the expander for the given in/out conditions. Here again, the mass-averaged values were applied. As the study involves a single-stage machine without diffuser, the total-to-static efficiency includes the contribution of the kinetic energy lost at the rotor outlet.

From the analysis of the results, the following issues were determined:

1) The power output calculated with the first-attempt 3D procedure (4,504 W) is about 10% lower than that resulting from the 0D design(5,093 W). This is due to the non-optimal guidance of the fluid by the blade, which leads to a positive average mass-averaged value of the angle of deviation at rotor output (thus resulting in a power loss based on Euler's equation [16]). The relevant error on c_3 is also due to the difference in the tangential component.

2) The shape of the meridional channel induces a heavy reduction of the velocity (diffusion) in the middle of the channel zone, close to the hub surface (figure 5).

3) Observing the Blade Loading diagram comparison in the blue lines of Figure 5 (first-attempt geometry; Figure 5 shows the pressure profiles on the SS and PS along the non-dimensional meridional coordinate), the hub region is clearly lightly loaded, with small differences between Pressure Side and Suction Side pressure

distributions. Moreover, along the entire blade height, it is highlighted an unsatisfactory overlapping of the pressure distributions in the LE zone.

5. Results of the *improved* 3D design

In order to improve the above unsatisfactory aspects related to the first attempt 3D design of the rotor, mainly attributable to the fluid behaviour through the machine, some modifications to the impeller geometry were considered. The first-attempt design showed a non-optimal guidance of fluid. This significantly affects the power output (7), because it determines a relatively large tangential component of absolute velocity at the TE (c_{u3}). For this reason, the number of blades was increased from 8 to 10. Another relevant aspect is the shape of the meridional channel; the first attempt geometry produced an unsatisfactory expansion of the fluid, especially in the near-hub zone where some recirculation and very low velocities were noticed. Therefore, the shape of the meridional channel and the distribution of β and Θ angles were modified (Figure 6). Figure 7 shows the improved geometry of the impeller.

Observing the blade loading for the improved geometry (red lines in figure 5) it is clear that a large fraction of load is re-located at the central part of the profile, on each of the considered layers (10%, 50% and 90% span). In addition, the rapid increase of velocity on the Suction Side (shown in Figure 5, 50% span) implies that the largest fraction of pressure drop is already achieved at about 40% of the camber line; this effect is emphasized approaching the shroud region. As it can be seen, with respect to the first-attempt Blade Loading curves (blue lines), a better work extraction in the near-hub zone is achieved. Furthermore the load has a more homogeneous distribution along the blade's height, which is important in order to limit secondary flow effects.

The contours of relative velocity at 50% blade height are reported in Figure 8. A local recirculation along the first 20% of the pressure side is noticeable; while in the first part of the suction side, high values of relative velocity were registered, which are due to the high profile curvature in this zone. The maximum relative Mach number inside the vane is about 0.54.

A qualitative assessment of the improvement of the rotor design can be done comparing the Relative Mach (M_{rel}) distributions on meridional surface (Figure 9).

After the modification of the geometry it is possible to register a more satisfactory behaviour of the flow through the meridional channel, with a smoother expansion of the fluid from the inlet to the outlet and a removal of the aforementioned diffusion bubble in the near-hub zone. The main results of the modified geometry are summarized in table 6.

6. Comparison between 0D and 3D: Results and discussion

The last part of this work deals with the comparison between the overall results of the zero-dimensional design and those of the three-dimensional CFD (these last are obtained by mass-averaging the results of the flow computation on the inlet and outlet sections), both for the improved geometry. Table 7 shows the comparison between the most relevant parameters calculated with the 0D and 3D CFD models, both related to the improved geometry.

On the whole, the significant calculated parameters are in fair agreement for the two approaches. It is interesting to compare the absolute velocities calculated at the leading and trailing edge sections. A lower agreement was found for the magnitude of the absolute velocity c_3, which is slightly higher in the 3D design. The isentropic total-to-static efficiency shows a very satisfactory agreement, with a 0D – 3D relative error within 1,5%. Finally, the two models predict close values of power output, with a relative error less than 5%.

7. Conclusions

Starting from a previously developed OD design tool for radial ORC expanders [14], specifically tuned on a 50 kW machine and able to account for the specific loss correlations across the rotor, a 3D design procedure for very small expanders (power rating 5 kW) was developed with the purpose of achieving an improved design, mainly concerning the geometry of the flow channel and the number of blades.

The results of the 0D tool (requiring reduced computational time, thus very suitable to be used as a preliminary design) are the basis for the definition of the geometry of the expander. Compared to many existing literature 3D models, the here developed one considered the real behaviour of the working fluid, by means of SRK EOS.

The 3D geometry of the rotor was imported in commercial CFD packages [21-24]. The 3D approach is applied at two different levels, first-attempt (the geometry is a simple outcome of the 0D design) and improved (the geometry is revised after a computer-assisted evaluation of the shortcomings of the first-attempt). The improved design corresponds to the final fluid dynamics design of the rotor, with the improved blade geometry and a more suitable number of blades (which is not directly provided by the traditional 0D correlations), determining a correct blade loading which is not achievable applying 0D design guidelines.

The results of the 0D and 3D models applied to the reference case (a 5 kW machine operating with R134a) showed a satisfactory agreement, confirming the reliability of the 0D design tool as the basis for the definition of the overall geometry and working parameters of the machine. The coupling of the two approaches appears to represents a reliable design procedure for small and micro radial turbines working with organic fluids in ORCs.

Nomenclature

a_f	Acentric factor
b	blade height [m]
c	absolute velocity [m/s]
d	diameter [m]
h	enthalpy [J/kg]
k	Turbulence kinetic energy [J/kg]; Thermal Conductivity [W/m-K]
Ma	Mach number
$\dot{m}$	mass flow rate [kg/s]
M_w	Molecular Weight [kg/kmol]
N_s	specific rotational speed [rpm]
p	pressure [Pa]
P	power output [kW]
r	radius [m]
R	Degree of reaction
T	temperature [K]
u	peripheral velocity [m/s]
V_{sound}	sound speed [m/s]
v	Specific volume [m^3/kg]
w	relative velocity [m/s]
Z	number of blades of the rotor

<u>Greeks</u>

α	Absolute flow angle (from radial direction, positive in the u direction) [°]

β	Blade Angle; Relative flow angle (from radial direction, positive in the u direction) [°]
Δ	Variation
ξ	Loss coefficient
η	Efficiency
Θ	Blade Wrap angle [°]
μ	Dynamic viscosity [Kg/s-m]
ν	Kinematic viscosity [m^2/s]
ρ	Density [kg/m^3]
Φ	Flow coefficient
Ψ	Load coefficient
ω	Specific dissipation rate
Ω	Angular velocity [rpm]

Subscripts/Superscripts

0	total value (stagnation)
1, 2, 3, 4	referred to sections 1, 2, 3, 4 (figure 1)
c	critical
D	diffuser
is	isentropic
m	meridional component
ts	total to static
u	peripheral
$-$	mass-average

Acronyms

CFD Computational Fluid Dynamics

IFR Inflow Radial (turbine)

NACA National Advisory Committee for Aeronautics

ORC Organic Rankine Cycle

References

[1] Vaja, I., Gambarotta, A., 2010, "Internal Combustion Engine (ICE) bottoming with Organic Rankine Cycles (ORCs)", *Energy,* 35 , 1084–1093.

[2] Schuster, A., Karellas, S., Kakaras, E., Spliethoff, H., 2009, "Energetic and economic investigation of Organic Rankine Cycle applications", *Applied Thermal Engineering*, 29, 1809–1817.

[3] Zhai, H., Dai, Y.J., Wu, J.Y., Wang, R.Z. , 2009, "Energy and exergy analyses on a novel hybrid solar heating, cooling and power generation system for remote areas", *Applied Energy*, 86 , 1395–1404.

[4] Fiaschi, D., Lifshitz, A., Manfrida, G., Tempesti, D., 2014, "An innovative ORC power plant layout for heat and power generation from medium- to low-temperature geothermal resources", *Energy Conversion and Management*, 88, 883-893.

[5] Di Pippo, R., 2006, "GeothermalPower Plants: Principles, Applications and Case Studies", *Elsevier Advanced Technology*, London, UK.

[6] Heberle, F., Brüggemann, D., 2006, "Exergy based fluid selection for a geothermal Organic Rankine Cycle for combined heat and power generation", *Applied Thermal Engineering,* 30, 1326-1332.

[7] Lentz, A., Almanza, R., 2006, "Solar–geothermal hybrid system", *Applied Thermal Engineering*, 26, 1537–1544.

[8] Dai, Y., Wang, J., Gao, L., 2009, "Parametric optimization and comparative study of organic Rankine cycle (ORC) for low grade waste heat recovery", *Energy Conversion and Management*, 50, 3, 576-582.

[9] Dong, L.L., Liu, H., Riffat, S.B., 2009, "Development of small-scale and micro-scale biomass-fuelled CHP systems" - A literature review, *Applied Thermal Engineering*, 29, 2119-2126.

[10] Qiu, G., Liu, H., Riffat, S., 2011, “Expanders for micro-CHP systems with organic Rankine cycle”, *Applied Thermal Engineering*, 31, 16, 3301-3307.

[11] Song, P., Wei, M., Shi, L., Syed Noman Danish, Chaochen Ma, 2015 “A review of scroll expanders for organic Rankine cycle systems”, *Applied Thermal Engineering*, 75, 22, 54-64.

[12] Rahbar, K., Mahmoud, S., Al-Dadah, R.K., 2014, “Mean-line modeling and CFD analysis of a miniature radial turbine for distributed power generation systems”, *International Journal of Low-Carbon Technologies*, 0, 1–12.

[13] Rahbar, K., Mahmoud, S., Al-Dadah, R.K., Moazami, N., 2015, “Modelling and optimization of organic Rankine cycle based on a small-scale radial inflow turbine”, *Energy Conversion and Management,* 91, 186–198.

[14] Fiaschi, D., Manfrida, G., Maraschiello, F., 2015 “Design and performance prediction of radial ORC turboexpanders”, *Applied Energy*, 138, 517-532.

[15] Micheli, D., Reini, M., 2007, “On bottoming a micro turbine with a micro ORC section: Part a) preliminary design of the ORC expander”, Proceedings of *ECOS Conference, Padova,* 1025-1033.

[16] Dixon, S.L., 1998, “Fluid Mechanics and Thermodynamics of Turbomachinery”, Fifth Edition, *Elsevier Butterworth-Heinemann*.

[17] Whitfield, A., Baines, N.C., 1990, "Design of Radial Turbomachines", *Longman Scientific and Technical*.

[18] Rohlik, H. E., 1975, "Radial Inflow Turbines," NASA SP 290, Vol. 3, Ch. 10.

[19] Matsuura, K., Kato, C., Yoshiki, H., Matsuo, E., 2003, “Prototyping of Small-sized Two-dimensional Radial Turbines”, *IGTC Tokyo*, 1–7.

[20] Aghaali, H., Hajilouy-Benisi, A., 2008, “Experimental modeling of twin-entry Radial Turbine”, *Iranian Journal of Science and Technology*, 32, 571–584.

[21] ANSYS Inc., 2011, “ANSYS TurboSystem User's Guide”.

[22] ANSYS Inc., 2011, “ANSYS TurboGrid User’s Guide”.

[23] ANSYS Inc., 2011, “ANSYS FLUENT Theory Guide”.

[24] ANSYS Inc., 2011, “ANSYS FLUENT User’s Guide”.

[25] Soave, G., 1972, “Equilibrium constants from a modified Redlich–Kwong equation of state”, *Chemical Engineering Science,* 27, 1197-1203.

Figures captions

Figure 1 – Sketch of the expander (meridional section)

Figure 2 – Share of rotor losses of the 5 kW expander

Figure 3 - Impeller 3D geometry

Figure 4 - Rotor computational grid (single sector, one blade passage and refined zones)

Figure 5 - Blade loading curves comparison for first-attempt and improved profiles

Figure 6 – Distributions of the angles for the two geometries

Figure 7 - impeller 3D improved geometry

Figure 8 – Distribution of relative velocity (Midspan layer, Improved geometry)

Figure 9 – Relative Mach Number distribution on meridional surface

Tables captions

Table 1 – Main input data of the 5 kW expander

Table 2 – Main 0D design results of the 5 kW expander

Table 3 - Physical properties of R134a working fluid

Table 4 - CFD design main results - first attempt geometry

Table 5 - Comparison between 0D design and 3D CFD design for initial geometry

Table 6 - CFD design main results - improved geometry

Table 7 - Comparison between 0D design and 3D CFD design for improved geometry

Figures

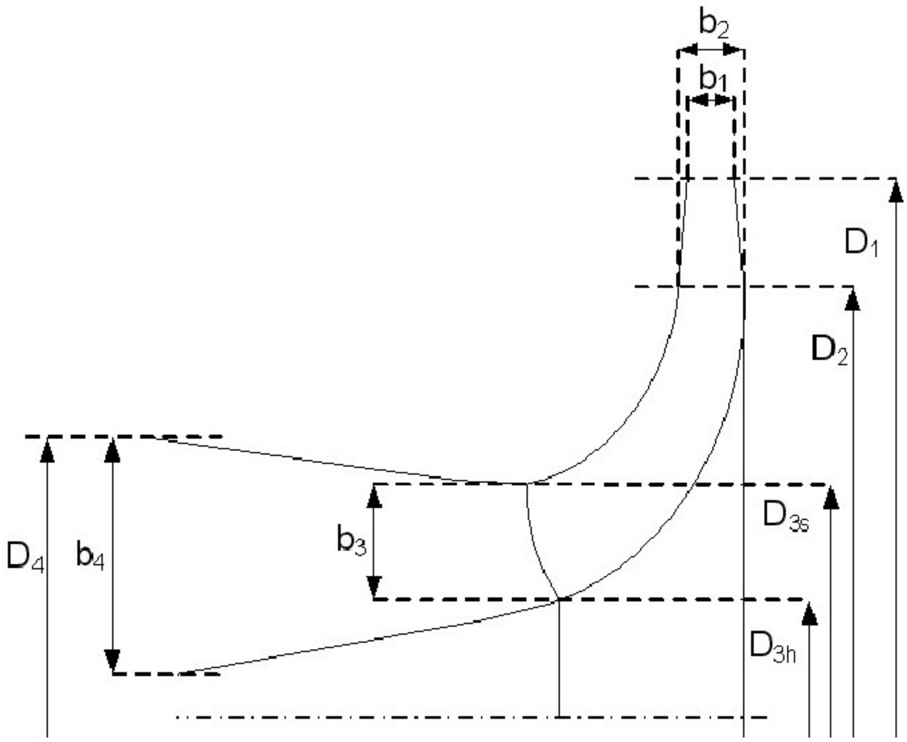

Figure 1

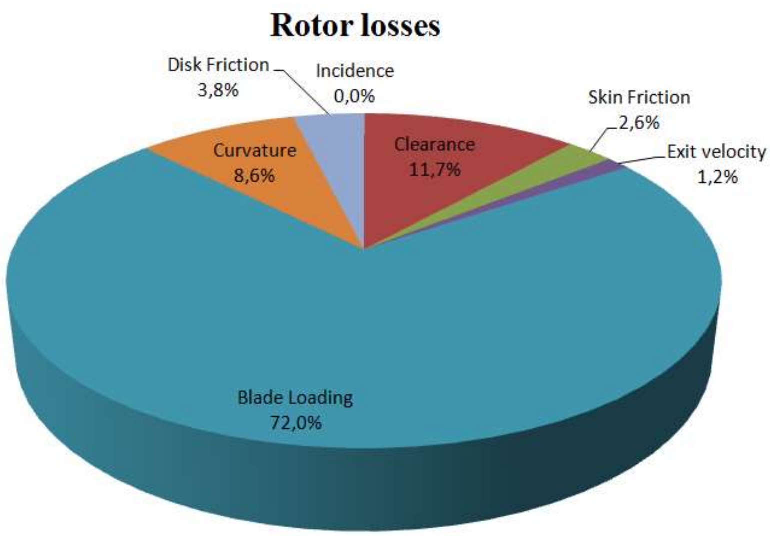

Figure 2

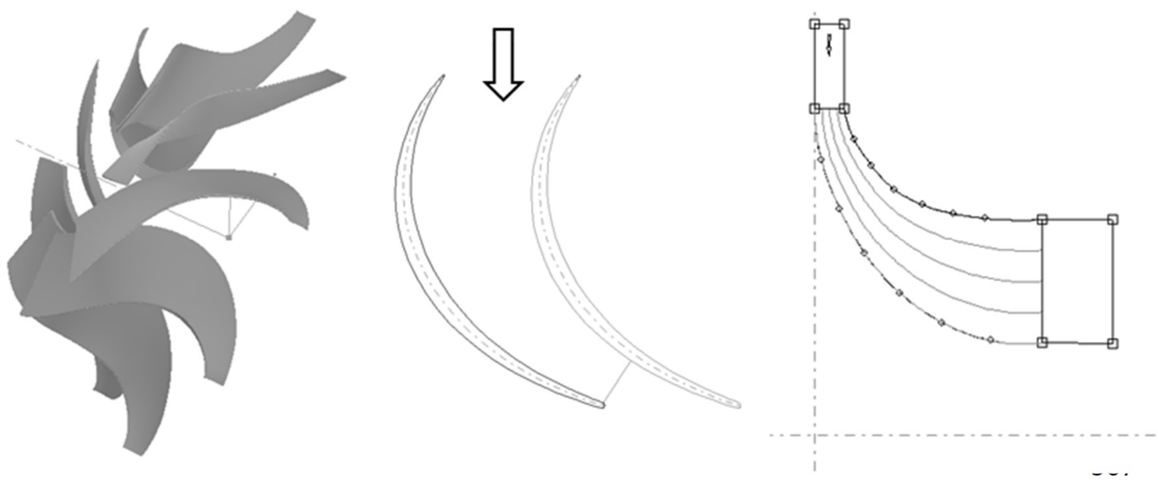

Figure 3

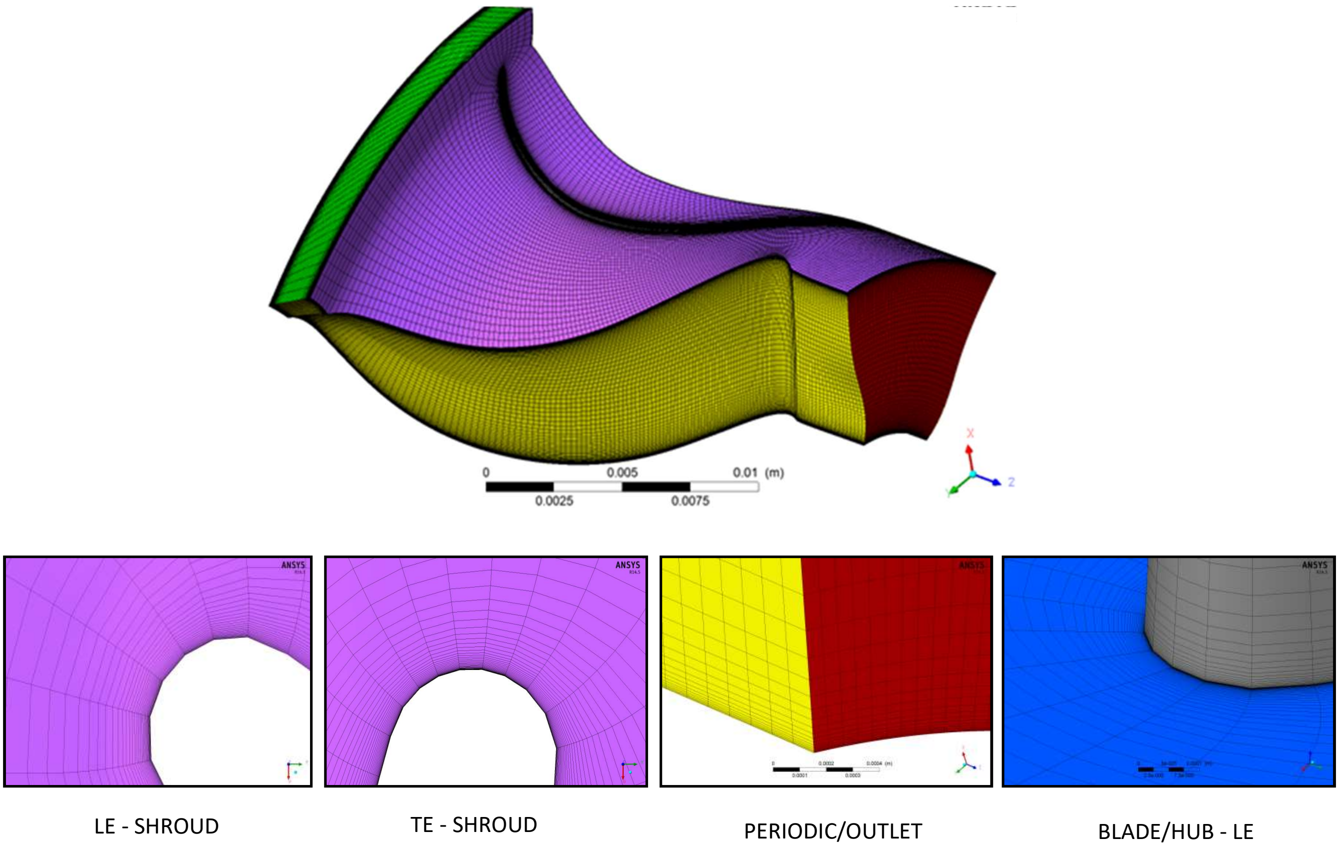

Figure 4

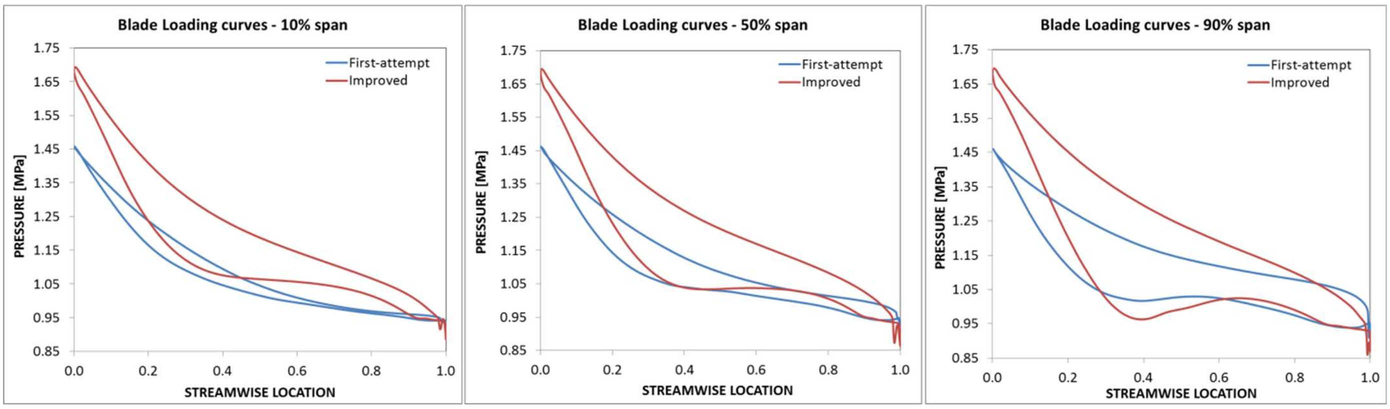

Figure 5

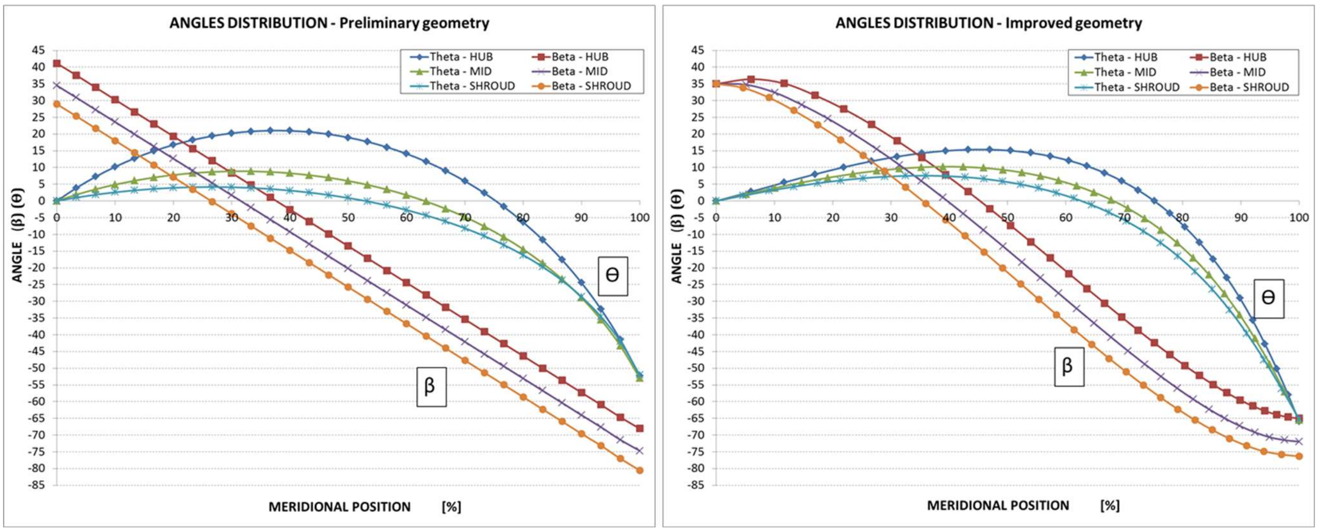

Figure 6

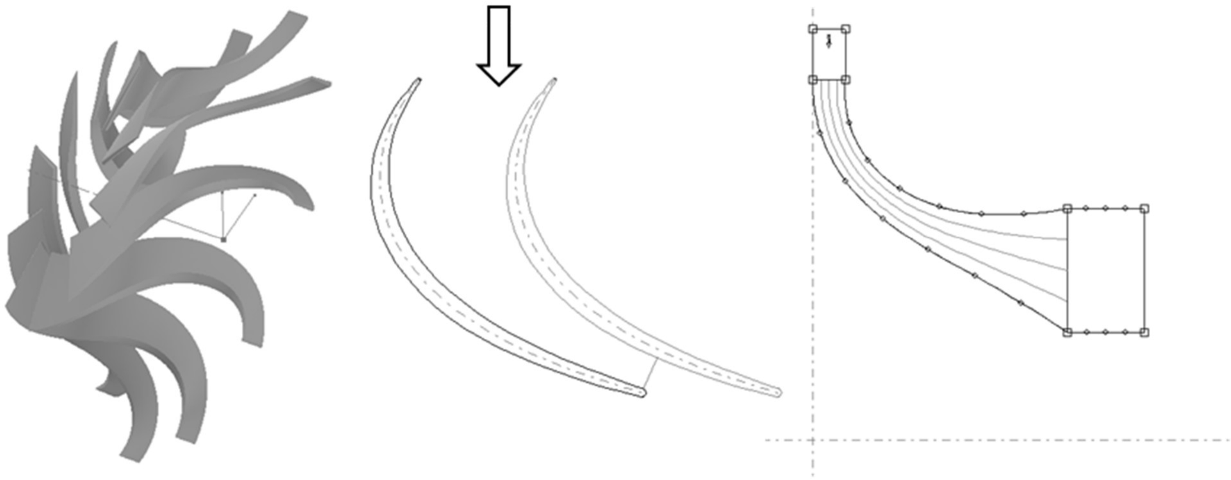

Figure 7

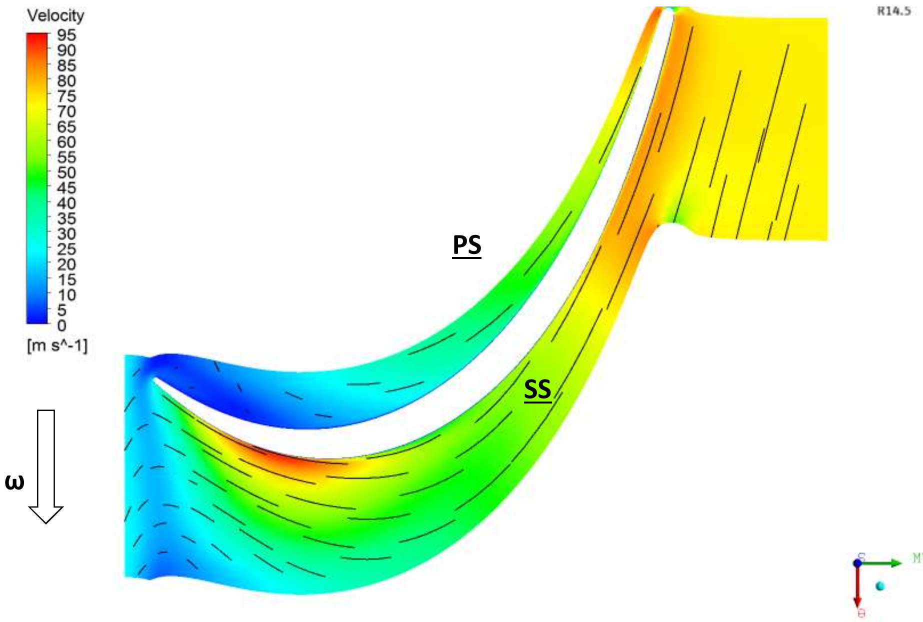

Figure 8

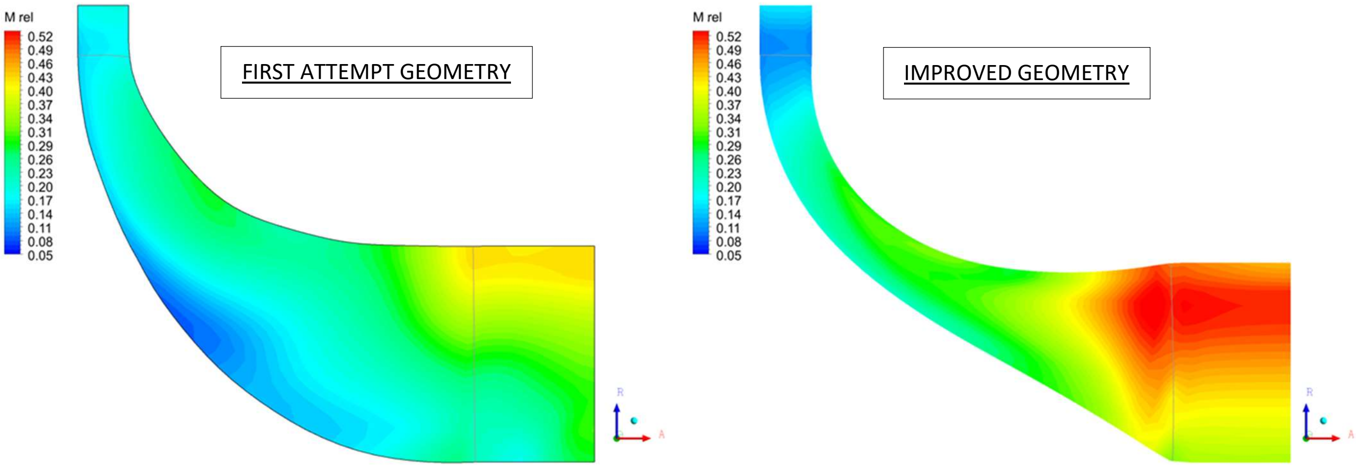
M rel
0.52
0.49
0.46
0.43
0.40
0.37
0.34
0.31
0.29
0.26
0.23
0.20
0.17
0.14
0.11
0.08
0.05
FIRST ATTEMPT GEOMETRY
M rel
0.52
0.49
0.46
0.43
0.40
0.37
0.34
0.31
0.29
0.26
0.23
0.20
0.17
0.14
0.11
0.08
0.05
IMPROVED GEOMETRY

Figure 9

Tables

Parameter	*Value*	*Unit*
	Non-dimensional (Flow)	
Ψ	0.995	[-]
Φ	0.09	[-]
R	0.63	[-]
	Dimensional	
d_2	0.035	[m]
p_{01}	3.8	[MPa]
T_{01}	420.15	[K]
	Non-dimensional (Geometry)	
d_1/d_2	1.45	[-]
d_3/d_2	0.47	[-]
d_4/d_3	1.4	[-]
L_D/D_3	1.5	[-]
b_2/d_2	0.0452	[-]
b_1/b_2	1	[-]

Table 1

Parameter	*Value*	*unit*
Power output *(P)*	5093	[W]
Mass Flow Rate *($\dot{m}$)*	0.1984	[kg/s]
Angular velocity *(Ω)*	87,645	[rpm]
Number of rotor blades Z_B	8	
Isentropic enthalpy variation *(Δh_{stage})*	37,000	[J/kg]
Absolute velocity inlet angle *(α_2)*	84.8	[°]
Relative velocity inlet angle (β_2)	-3.2	[°]
Global rotor loss coefficient *(ξ_R)*	3.409	[-]
Total to Static efficiency *(η_{ts})*	0.6935	[-]
c_2	160.5	[m/s]
c_3	19.93	[m/s]
w_2	14.48	[m/s]
w_3	78.08	[m/s]
u_2	160.6	[m/s]
u_3	75.49	[m/s]
V_{sound2}	160.8	[m/s]
V_{sound3}	168.7	[m/s]
Ma_{r2}	0.090	[-]
Ma_{r3}	0.463	[-]
p_{02}	3.673	[MPa]
p_2	2.251	[MPa]
p_{03}	0.9409	[MPa]
p_3	0.9341	[MPa]
ρ_2	84.85	[kg/m^3]
ρ_3	33.97	[kg/m^3]
T_2	122.9	[°C]
T_3	97.53	[°C]

Table 2

Physical property	***Value***	***unit***
Specific Heat (c_p)	1,109	[J/kg-K]
Thermal Conductivity (k)	0.02065	[W/m-K]
Dynamic viscosity (μ)	$1.553e^{-5}$	[kg/s-m]
Molecular Weight (M_w)	102	[kg/kmol]
Reference Temperature (T_{ref})	298.15	[K]
Critical Temperature (T_c)	374.2	[K]
Critical Pressure (p_c)	4.059	[MPa]
Critical Specific Volume (v_c)	0.001969	[m^3/kg]
Acentric Factor (a_f)	0.3269	[-]

Table 3

Variable	***CFD***	***unit***
$\dot{m}$	0.1984	[kg/s]
η_{ts}	68.04	[%]
P	4,504	[W]
p_2	1.45	[MPa]
p_{02}	2.32	[MPa]
p_3	0.950	[MPa]
p_{03}	0.970	[MPa]
T_{02}	395.9	[K]
T_{03}	368.6	[K]
h_{02}	345,300	[J/kg]
h_{03}	322,600	[J/kg]

Table 4

Variable	***unit***	***0D design***	***3D CFD first attempt design***	***0D – 3D relative error [%]***

c_2	[m/s]	160.5	158.3	-1.4
c_3	[m/s]	19.9	36.7	45.8
η_{ts}	[%]	69.90	68.04	-1.86
P	[W]	5,093	4,504	-11.6

Table 5

Variable	***CFD design***	***unit***
$\dot{m}$	0.2013	[kg/s]
η_{ts}	71.76	[%]
P	5,162	[W]
Z_B	10	
p_2	1.67	[MPa]
p_{02}	2.87	[MPa]
p_3	0.94	[MPa]
p_{03}	0.95	[MPa]
T_{02}	399.4	[K]
T_{03}	362.2	[K]
h_{02}	342,990	[J/kg]
h_{03}	317,348	[J/kg]

Table 6

Variable	***unit***	***0D Design***	***3D CFD Improved design***	***0D – 3D relative error [%]***
c_2	[m/s]	162.3	166.0	2.2
c_3	[m/s]	21.7	26.8	19.0
η_{ts}	[%]	72.78	71.76	-1.42
P	[W]	5,422	5,162	-4.8

Table 7